The UH-Nuclei Cosmic Ray Detector on the Third High Energy Astronomy Observatory

W.R. Binns, M.H. Israel, J. Klarmann, W.R. Scarlett,
E.C. Stone, and C.J. Waddington

Accepted for Publication
Nuclear Instruments and Methods

January, 1981

(81-6)

The UH-Nuclei Cosmic Ray Detector on the Third High Energy Astronomy Observatory

by

W.R. Binns,[1] M.H. Israel,[2] J. Klarmann,[2] W.R. Scarlett,[3*]
E.C. Stone,[4] C.J. Waddington[3]

[1]McDonnell Douglas Research Laboratories, St. Louis, MO 63166 (Present address: 2)

[2]Department of Physics and the McDonnell Center for the Space Sciences, Washington University, St. Louis, MO 63130

[3]School of Physics and Astronomy, University of Minnesota, Minneapolis, MN 55455

[4]Downs Laboratory of Physics, California Institute of Technology, Pasadena, CA 91125

*Present address: Los Alamos Scientific Lab, NM 87545

Abstract

The third High Energy Astronomy Observatory satellite (HEAO-3) carries a particle telescope for the detection of highly charged cosmic ray nuclei. These nuclei, which have $Z \gtrsim 28$, are much rarer than the lower charged nuclei in the cosmic radiation. As a consequence, this particle telescope was required to have a large collecting area as well as an ability to resolve individual elements. This paper describes the telescope, composed of large area parallel plate ionization chambers, multi-wire ion chamber hodoscopes and a Cherenkov radiation detector. The resulting telescope has a total geometry factor of 59,000 $cm^2 sr$ and is capable of measuring the charges of nuclei in the range $14 \lesssim Z \lesssim 120$.

1. Introduction

This paper describes the design and function of a detector of UH or ultra-heavy cosmic ray nuclei, which was flown on the HEAO-3 spacecraft launched into near-earth orbit on September 20, 1979. This instrument was designed to make observations with good charge resolution and high statistical weight on the elemental abundances of those cosmic ray nuclei that have atomic numbers, Z, significantly greater than that of iron, Z = 26. These UH-nuclei are relatively rare in the cosmic radiation, having abundances four to six orders of magnitude less than those of the nuclei in the iron charge region. Consequently, it has been difficult to accumulate a statistically adequate sample of UH-nuclei and those samples that have been obtained have suffered from rather poor experimental charge resolution, inadequate to distinguish individual elements.[1,2] The astrophysical significance of observations on the UH-nuclei has been reviewed by Israel et al.,[3] but in every case must be greatly improved by measurements with a capability of resolving individual elements. These nuclei represent a sample of matter that has had a unique history, and a knowledge of their abundances should allow us to examine both the nucleosynthesis processes that are responsible for the creation of these heavy elements, and the acceleration mechanisms that produce the cosmic radiation. Similarly, the propagation of cosmic ray nuclei in the interstellar medium will be most sensitively probed by examining these heavy elements.

Our current knowledge of the abundances of these nuclei has been summarized by various groups,[1,4] but there is still considerable uncertainty regarding even the gross features of the abundance distribution. For example, Meyer[5] has recently suggested that the abundances of the actinides, those elements with $89 \leq Z \leq 103$, may be as much as a factor of three less than previously claimed, which would seriously affect the interpretation of these abundances in terms of theories of

nucleosynthesis. Similar uncertainties affect our understanding of the origin and significance of the intermediate charged nuclei.

It has been clear for a long time that these uncertainties would be significantly reduced by a long duration space exposure of a large detector capable of resolving the individual elements. In about 1970 we made various proposals to NASA for such exposures on the High Energy Astronomy Observatory series of satellite missions. The resulting detector array described in this paper is an amalgamation of our several proposals that has been optimized to the configuration of the HEAO-3 spacecraft.

In our design of this detector, we have had two major requirements. Firstly, as an overriding factor, we have required that the detector system should be capable, in principle, of resolving individual elements over the range $17 \lesssim Z \lesssim 100$, and, secondly, that the collecting power or geometry factor, the area-solid-angle product, be as large as physically possible. These two requirements have affected the design at every stage of development, from the initial selection of the basic detector types, to the selection of details such as the wire spacing of the hodoscopes.

In order to meet the charge resolution requirement, it was necessary to select detector elements that we could reasonably expect to produce signals that were linearly related to the energy loss, even in a charge region in which there was little or no prior experimental data. Thus, while some types of detectors, such as plastic or crystalline scintillators, produce signals that are nonlinear with increasing energy loss even at charges as low as $Z \approx 26$, we required detectors that would have a good probability of a linear, or at least smoothly increasing, response up to $Z \gtrsim 100$. A further consideration in any selection of a detector type came from the wide energy range of the particles that any space mission would encounter, so that both Z and the reduced velocity β ($\beta = v/c$) have to be

determined for each particle, which in general requires at least two different measurements. Conventionally, high energy cosmic ray detector arrays have used a measure of ionization energy loss, dE/dx, which varies as $Z^2/\beta^2 \cdot f(\beta)$, combined with a measure of Cherenkov energy loss, which varies as $Z^2(1 - \frac{1}{\beta^2 n^2})$, where n is the refractive index. Such a combination is generally, though not always, sufficient to define both Z and β uniquely. At low latitudes, where the geomagnetic field cutoff ensures that all the incident nuclei have $\beta \cong 1$, measurements of dE/dx and C provide essentially independent measurements of Z.

These considerations led to a detector array in which we measure the ionization energy loss by using a parallel plate gas-filled ionization chamber of a type similar to those developed by Epstein et al.[6] for use in balloon flights. Such chambers have the advantages of introducing very little matter into the trajectory of the particles, which therefore have only a small probability of suffering a nuclear interaction while they traverse the detector; of having a nearly linear response to energy loss even for ionization densities larger than those expected from the highest charged cosmic ray nuclei; and of not requiring accurately controlled bias voltages. Their principal disadvantage is the relativistic rise of the signal as the energy increases above several GeV/nucleon, which is a larger effect in a gas than in a solid medium. As a result, for many of the detected nuclei Z is a double-valued function of the instrument response. In addition, there is the practical disadvantage that a pressure vessel is required to maintain the gas at a pressure of about one atmosphere. The Cherenkov energy loss is determined using plastic radiators mounted in a light diffusion box viewed by photomultiplier tubes (PMT) which measured the integrated light intensity produced in the radiators by the passage of nuclei.

These charge measuring detectors, when combined with multi-wire ionization chamber hodoscopes to define particle trajectories, make up the HEAO-3 detector array.

The HEAO-3 spacecraft was launched into a circular orbit with initial altitude 496 km and inclination 43.6 degrees. During the first 9 months of operation the spacecraft spun about its Z axis with a 20 minute period. Our instrument is oriented with its principal viewing directions along the spacecraft's Y axis. Since the spin axis is oriented toward the Sun (or toward some other celestial point within 30° of the Sun), the instrument does not have a fixed orientation with respect to the Earth; however, star sensors on the spacecraft provide post-facto attitude determination to better than 0.5°.

2. Physical Description

A schematic of the detector array (Fig. 1) shows that the array is composed of two modules which when combined make a system symmetric about the x-z plane that responds to particles entering from either side of this plane. A particle penetrating the entire array from "above" will encounter successively a hodoscope, H1, which gives two coordinates; three ion chambers, each with separate pulse height analyzers (PHA); another hodoscope, H2; two layers of Cherenkov radiator, the combined light from which is viewed by eight photomultiplier tubes, each of which has a separate PHA; a hodoscope, H3; three ion chambers; and a final hodoscope, H4. Such events, designated as H1·H4 events, have a geometry factor of 1.12 m^2sr and are clearly those with the highest obtainable charge resolution.

In operation, the requirement for an event was not nearly as restrictive, but instead was generally that the particle trigger at least two of the seven

charge measuring detectors and at least two of the four hodoscopes (see Sect. 3.4 for variations in this basic trigger requirement). The resulting total geometry factor is 5.9 m^2sr, made up of the various different classes of events. The different integral and differential geometry factors, expressed as a function of the angle with respect to the instrument axis, are shown in Figures 2a and b, where these factors are calculated from a numerical integration and confirmed with totals calculated from the analytical expressions of Sullivan.[7] Not all of the total geometry factor is useful at all times. For example, 32% of the $H1 \cdot H2 \cdot \overline{H3}$ or $H4 \cdot H3 \cdot \overline{H2}$ particle trajectories miss both Cherenkov radiators. It is possible to assign a charge to such particles only if the geomagnetic cutoff is greater than about 5 GV, which is the case for some 70% of all those observed, and even then only with reduced confidence.

2.1 Gas Detectors

The two rectangular pressure vessels each contain two hodoscopes and three ionization chambers. Each dual-gap ionization chamber consists of a central anode mounted midway between two cathodes, with anode to cathode spacing of 6.9 cm. These electrodes are aluminum screen-wire stretched in a frame of aluminum channels, and look rather like standard window screens. The electrodes are basically rectangular, 155.6 cm x 125.1 cm. Aluminum frames take the outermost 2.5 cm of this rectangle, and the remainder is unsupported screens woven of 0.025 cm diameter aluminum wires, spaced 6.3 per cm. The mean areal density of each screen is 0.02 g/cm^2. The screens are attached to the frames under sufficient tension to bow the frames inward about 1 cm at the center of each side, thus ensuring that the screens remain flat. Fourteen insulated stainless steel posts spaced along the perimeter support all the electrodes and maintain their spacing.

Each hodoscope consists of two layers, giving x- and z-coordinates. Each layer has an anode plane composed of discrete parallel wires (0.025 cm diameter stainless steel) spaced 1 cm apart; the anode plane is midway between two screen-wire cathodes, identical to the ionization chamber electrodes. The anode-cathode spacing in the hodoscope is 1.0 cm. The theory and operation of a similar multi-wire ionization hodoscope has been described by Love et al.[8]

Each pressure vessel has top and bottom windows made of aluminum honeycomb 8.9 cm deep, with mean areal density of 1.2 g/cm^2. The side walls are 0.32 cm thick aluminum with 5.1 cm deep aluminum ribs on the outside. Electronic packages are mounted on the sides between the ribs. The cosmic ray nuclei that enter through a side wall (45% of the total 5.9 m^2sr geometry) penetrate various amounts of material, typically 2 to 3 g/cm^2. While these side-entering events are thus of lower quality than window-entering events, they are essential for maximizing our geometry. Similarly, a rectangular shape for the pressure vessel was chosen to maximize the geometry within the constraints imposed by spacecraft despite the fact that it required thicker windows than would a cylindrical design.

The gas inside the pressure vessels is 90% argon, 10% methane (P-10). A trace ($\sim$0.5%) of helium was added to facilitate leak checking; this helium had no signficant effect on the ionization characteristics. The gas pressure is slightly greater than one atmosphere absolute (838 torr at 20°C). These vessels are sealed and have no make-up gas supply in the spacecraft. The resulting requirement that the gas maintain the necessary purity for several years required careful selection of materials and cleaning procedures, which are discussed in the next section.

2.2 Gas Quality Tests

The inherent difficulties of providing an onboard gas supply capable of refilling or flushing the ion chamber/hodoscope detectors in case of gas degradation made it desirable to develop sealed ion chambers that could operate for a long time without showing significant changes in characteristics. For this reason, it was necessary to ensure that thermal or radiation induced outgassing of the materials used in the construction of the ion chambers would not degrade the detector performance over a period at least equal to the maximum expected HEAO-3 lifetime. A small test ion chamber similar to the flight chamber was constructed in order to test the various materials used. This chamber was a dual gap chamber with screen electrodes of the same type and with the same spacing as those in the flight instrument. A ^{252}Cf source was mounted in the chamber to act as a source of constant amplitude signals to monitor the ionization-chamber response to charged particles. Materials used in the flight chamber construction were initially selected on the basis of their low outgassing properties, and those judged likely to outgas any electronegative contaminates were particularly avoided.

Table I lists all the materials tested including some materials not used in flight chamber constructions. The chamber was irradiated four different times with various combinations of materials included for each test. Two of these tests used 25 MeV electrons (Washington University Clinac 35 electron accelerator) at a dose of 5×10^4 rads; and two utilized 600 MeV protons (Space Radiation Effects Laboratory proton cyclotron) at a dose of 10^4 rads. The calculated in-flight dose received by materials inside the HNE ion chambers is ~450 rads, primarily due to exposure to protons in the South Atlantic

Anomaly (SAA). Since electrons are only about 1% as effective in producing damage in solids as protons (for the above energies), the effective test electron dose is about equal to, and the test proton dose a factor of 20 greater, than that expected in orbit. After each irradiation, the chamber was monitored for a period of a year or longer. The results of these tests were that no significant degradation (>1%) in signal was observed to occur for any of the listed materials (Table I) and they could therefore be used in ion chamber construction. Flight data has confirmed these test results, since the chambers were sealed in February 1978, launched September 30, 1979, and have performed with no observable change.

2.3 Ionization Chamber Operation Parameters

The ionization chamber operating pressure was chosen so that ionization statistics would be sufficient for the combination of three ionization chamber measurements to give an overall charge resolution of $\sigma = 0.3$ charge units for minimum ionizing iron nuclei.

The operating voltage for the ionization chambers is -1000 V with electrode spacing 6.9 cm. The operating voltage was chosen on the basis of two considerations. The first was that the electron drift velocity be on the drift velocity plateau so that small changes in pressure or voltage would not significantly alter the chamber electron collection characteristics. The broad peak in the drift velocity curve for P-10 gas taken from English and Hanna[9] is at E/p = 120 V/(m·kPa) and is plotted as a dashed line in Figure 3. The operating E/p is 128 V/(m·kPa), providing an adequate margin for small pressure or voltage changes.

The second consideration in the choice of operating voltage was the requirement that electron collection losses must be small for even the most

densely ionizing nuclei expected in this experiment. To determine the voltage necessary to satisfy this requirement, a laboratory experiment was performed utilizing a three electrode, gridded (Frisch) ion chamber with fission fragments and alpha particles from a ^{252}Cf radioactive source as the ionization source. Curves A and B in Fig. 3 show the peak signals of the alpha distribution (E_α = 6.1 MeV) and the most energetic fission fragment distribution[10] (E_F = 102 MeV) for a P-10 gas pressure of 107 kPa (800 torr). At the operating E/p, the alpha curve exhibits essentially no electron loss (dE/dx of the alphas is approximately equivalent to a 300 MeV/amu, Z = 17 nucleus) but the fission fragment curve indicates electron losses of ~3%. The fact that electron losses are more severe for large dE/dx indicates that nonlinear effects in dE/dx are operative. A simple model assuming electron-ion recombination (quadratic in dE/dx) as the primary loss mechanism results in qualitative agreement with these experimental results. Actual electron losses for relativistic cosmic rays should be less than 3% however, since the average dE/dx for ^{252}Cf fission fragments is ≈3 times that of a 300 MeV/amu, Z = 100 nucleus. In addition, the fission fragment volumetric ionization density is even greater because the maximum energy it can transfer to a secondary electron is small (≈ 1 keV) compared to that of a 300 MeV/n nucleus (≈ 800 keV). A linear scaling of the α and fission fragment results according to dE/dx would indicate ≈1% losses, whereas a quadratic scaling gives ≅ 0.3%. Thus it is expected that electron collection losses for 300 MeV/amu, Z = 100 nuclei will be ≲1%.

2.4 Cherenkov Chamber

The top and bottom of the Cherenkov chamber are formed by the outsides of the adjacent ion chamber pressure vessel covers. The Cherenkov chamber side

walls are an extension of one of the pressure vessel covers and mate with a flange on the other pressure vessel to form a light-tight chamber when the two pressure vessels are mounted in the spacecraft. The radiators, one mounted on each of the pressure chambers, are 24.7 cm apart. A photomultiplier assembly (PMA) containing two EMI 9791NA 5-inch photomultiplier tubes, high voltage power supplies, preamplifiers and precision pulse generators for calibration,are mounted in each corner. In order to accommodate these PMA's within the envelope of the array without reducing the dimensions of the gas detectors, it was necessary to remove the corners of the Cherenkov radiators, which therefore have a total area that is 11% less than that of the hodoscopes. Each 0.47 cm thick radiator of Pilot 425 was sandblasted in order to improve the uniformity of response, and its back, like the walls of the chamber, painted with Kodak white paint No. 6080 and supported by a 5 mm sheet of Dorvan. The response of this Cherenkov chamber to sea level muons ($Z = 1$) was measured before flight and was found to correspond to 3-4 photo-electrons. The response of small samples of radiator to iron nuclei accelerated at the Bevalac showed a simple secant Θ dependence out to 45° to better than 1% and a typical low level scintillation component. The uniformity of response obtained in flight is discussed in Sec. 4.

3. Electronics Description

Figure 4 is a simplified overall block diagram of the electronics. Each of the six ionization chambers and each of the eight photomultipliers has its own signal processing electronics that consists of an amplifier with charge-sensitive input stage, pulse height analyzer (PHA) with pseudo-logarithmic

transfer function, and discriminators. Each of the 1120 hodoscope wires is attached to an amplifier and a discriminator; encoding logic records the location of wires with signals above the discriminator level. Outputs of the PHA's and hodoscope encoding logic are stored in a set of output buffers which transfer data to the spacecraft telemetry system in a single pre-determined format. The various discriminator outputs and the status of the data buffers are used by the event control logic (Sec. 3.5) to decide when to initiate event analysis.

3.1 Ion Chamber Electronics

The chambers are operated in orbit with a fixed -1000 V DC on the cathodes. For test purposes on the ground only, the high voltage was externally adjustable to lower values because previous experience had demonstrated that at lower voltages the chamber is more sensitive to trace contaminants in the gas. During ground testing we routinely monitored the chamber response to the internal calibration sources for operating voltages over the range -400 V to -1000 V but saw no degradation from the time the chambers were first sealed through the last prelaunch check.

The amplifiers shape their input signal with two integrations and two differentiations, all with 2 μs time-constant. This shaping permits effective response to the electron component of the ionization, which is fully collected at the anode in 1.2 μs, but the positive ions, with drift velocity several thousand times slower, make negligible contribution to the analyzed signal. The resulting charge signal on the input of the amplifier is Ne/2 coulombs for collection of N electrons, each of charge e, uniformly produced along the

path of a cosmic ray nucleus traversing the chamber.[6] The input signal to the preamplifier for a vertically-incident iron nucleus (Z = 26) of about 2 GeV/amu is 76 fC. Since the energy-loss of such a nucleus in the gas of one chamber is calculated to be 25.2 MeV, this signal implies that the mean energy required to produce each electron is 26.6 eV, consistent with earlier published values.[11]

The input of the charge-sensitive preamplifier is a low-noise FET, 2N6453. The root-mean-square (rms) noise referred to input for the full linear system is 0.7 fC, derived from the Gaussian shape of the pulse-height distribution produced by the precision test pulses accumulated in orbit. For a single ionization chamber this noise contributes an rms error of 0.12 charge units to the signal of a minimum ionizing iron nucleus (Z = 26) with a trajectory perpendicular to the plates. For the mean of n chambers the rms charge error is reduced by $1/\sqrt{n}$, with n typically 3 to 6. For other nuclei the rms charge error varies as 1/Z and hence is negligible for UH-nuclei.

Each chamber has three discriminators set for signals at the preamplifier input of 29 fC, 125 fC, and 215 fC. The lowest of these three discriminators (designated LLD) is used in the basic event trigger logic. Its threshold is the signal expected of a minimum-ionizing sulfur nucleus (Z = 16) penetrating perpendicular to the electrodes. The intermediate and high level discriminators (designated ILD and HLD, respectively) have corresponding thresholds at Z = 33 and 44, and are used by the event control logic to identify events which are recorded on a priority basis (see Sec. 3.4).

The pulse height analyzers (PHA) have a pseudo-logarithmic response, characterized by the function

$$N = A \ln\left(\frac{Q}{B} + 1\right) + C$$

where Q = charge at preamplifier input

N = output channel number (maximum 4095). Typical values of the three parameters are:

A = 1215 B = 230 fC C = 55

For small signals ($Q << B$) the analyzer response is approximately linear at 0.2 fC/channel, while for large signals ($Q >> B$) the response is approximately logarithmic at 0.1%/channel. Full scale, approximately 6.2 pC, is approximately the signal expected from a nucleus of charge 126 and energy about 250 MeV/amu penetrating at 60° to the perpendicular. The ability to handle such high signals insures analysis of the highest-charged known elements, as well as any in the theoretically suggested islands of nuclear stability near Z = 114 and Z = 126. The constants of the pseudo-logarithmic function were selected to give channel widths that were approximately uniform with charge over the full range of interest. The channel width, expressed in terms of the nuclear charge of a minimum-ionizing nucleus penetrating perpendicular to the electrodes, is a minimum of 0.04 charge units for $Z \approx 50$ and rises slowly for lower or higher Z, reaching 0.06 charge units at Z = 18 and Z = 126. The analyzer response has proven to be very stable, with temperature coefficients less than 0.2 channels/degree C, a negligible effect since the temperature variations encountered by the pulse-height analyzers has been only 8°C.

To verify the stability of the linear electronics, a calibration pulser is built into the front end of each preamplifier. Precision pulses with eight different amplitudes are switched in turn onto a precision test input capacitor.

This calibration sequence runs at a low rate (0.19/sec) continuously pulsing all linear systems throughout the flight. For ground tests, the pulser voltage was externally controlled to permit calibration at many more pulse levels and at higher rates.

3.2 Cherenkov Electronics

Each of the eight PMT's has an independent high voltage supply which can be commanded to any one of thirty-one levels between about 1200 V and 1400 V. Each voltage step corresponds to a PMT gain change of approximately 8%. The operating voltages were selected to give nearly equal response from all eight PMT's to cosmic ray nuclei penetrating near the center of the Cherenkov counter, and to give the desired absolute signal on the pre-amplifier input. Care was taken to verify that the complete system was linear over the entire voltage range, with no measurable saturation effects.[12]

The signal at the pulse-height analyzer input for a nucleus of charge 26, $\beta = 1$, perpendicular to the radiators, is 20 pC at the PMT anode. Since such a cosmic ray nucleus causes the generation of approximately 250 photoelectrons from the cathode of each PMT, the PMT gain is approximately 5×10^5.

The Cherenkov signals are shaped in the same manner as the ion chamber signals using time constants of 1.9 μ sec. While the response time of the Cherenkov counter is very substantially shorter than this value, the slower response of the ionization chambers sets the instrument speed and there is no value to a higher Cherenkov electronics bandwidth, which would have resulted in increased noise. In fact, the Cherenkov electronic noise is negligible, 0.1 pC rms, contributing a rms error of 0.025 charge units at $Z = 26$ ($\beta = 1$), perpendicular) when the mean of eight PMT's is used to determine charge.

The discriminator on each PMT is set at 3.2 pC, approximately 16% of the signal of a perpendicular, $\beta = 1$, $Z = 26$, nucleus (or to the full signal of a corresponding nucleus of $Z \approx 10$). This discriminator is used in conjunction with the ionization chamber LLD's in the event-trigger logic and with the ILD's in determining priority events. This level is high enough to avoid signals from iron nuclei below the Cherenkov threshold which give signals due to scintillation and knock-on electrons at about 6% of the signal corresponding to $\beta = 1$. (The event logic actually uses a signal, called C2, which is generated by coincidence of Cherenkov discriminators on two PMT's not in the same corner of the instrument.)

The Cherenkov pulse height analyzers have a pseudo-logarithmic transfer function similar to those of the ionization chambers. Typical values of the constants are A = 1390, B = 61 pC, and C = 105. These values produce a dynamic range and nuclear digitization comparable to those of the ionization chambers with channel widths of 0.034 charge units at $Z \approx 46$, rising to 0.047 charge units at $Z \approx 20$ and 110 and a full scale at 870 pC when $\beta = 1$, $Z = 26$ gives 20 pC. A twelve-level in-flight calibration, carried out in conjunction with the ionization chamber calibration, has demonstrated slow gain drifts, with a typical range of variations of less than 0.3%.

3.3. Hodoscope Electronics

The hodoscope cathodes share the -1000 V high-voltage supply of the ionization chambers. With the 0.025 cm anode wire diameter the electric field strength is still low enough that the hodoscope works in the ionization mode, without gas gain.

Each anode wire is connected to the input of a charge-sensitive preamplifier. This preamplifier, a post amplifier, and a discriminator comprise a hybrid

circuit. The discriminator thresholds are set between 2.4 and 3.0 fC (referred to preamplifier input). The 3 fC threshold corresponds to the anode signal for Z = 16.2 in 1 cm of hodoscope gas. It should be noted that for the typical trajectory the path contributing to one anode is about 2 cm for which 3 fC corresponds to Z ≃ 11.5, but in the worst case, a nearly vertical trajectory midway between two anodes, the path contributing to each signal is indeed only 1 cm. Note also that for the electric field configuration of the hodoscope, the charge collection efficiency is 0.7 rather than the 0.5 value characteristic of plane parallel electrodes.[8] The electronic noise width of the discriminator thresholds is measured to be typically between 0.2 and 0.3 fC rms. This low noise is achieved by using 10 μs shaping time constants.

The locations of hodoscope wires which fired (i.e., gave signals above the discriminator threshold) are encoded in the following manner. There are eight layers of wires; four layers of 156 wires each, giving X-coordinates and four of 124 wires each, giving Z-coordinates. A typical cosmic ray nucleus traversing a layer should fire from one to eight adjacent wires, depending upon the angle of the trajectory. For each layer the instrument records the address (1 to 124 or 1 to 156) of the first (lowest address) fired wire and a seven-bit "pattern" representing the firing or non-firing of each of the next seven wires. Two such address/pattern combinations are recorded for each layer. For a normal event, only one address/pattern per layer would be required to describe it, but by recording two we ensure not only that a single discriminator malfunctioning in the "on" state does not block the recording of higher number wires, but also that if the effects of δ -rays produced by very high charge nuclei exceed the capacity of one address we still can record

the entire pattern. In addition, an overflow bit for each layer indicates if more wires fired than could be encoded in the two address/patterns.

Test inputs on each hodoscope preamplifier permit in-orbit testing at a single pulse level, as part of the normal electronic calibrate sequence. During ground test these levels were externally adjustable to test the discriminator levels and noise width.

3.4 Event Control Logic

The event control logic (ECL) utilizes inputs from discriminators on the various detectors to determine when an "event" has occurred, i.e., when a cosmic ray nucleus has traversed the detector within its acceptance geometry, and to determine whether an event is to be recorded as "normal" or "priority". If a data buffer (see Sec. 3.5) is available for recording this event, then the ECL issues signals to the pulse height analyzers and to the hodoscope encoding logic causing all fourteen PHA's to record pulse heights and all eight hodoscope layers to encode address/patterns. The standard event requirement is discriminator signals from at least two of the seven "charge detectors" and from two of the four hodoscopes. (The seven "charge detector" discriminators are the six ionization chamber LLD's, Sec. 3.1, and the Cherenkov C2, Sec. 3.2) A hodoscope discriminator output occurs if at least one wire fires in both the X and Z layers. The standard event requirement means that an event is analyzed whenever there is adequate information to determine a trajectory and to make two estimates of the nuclear charge, independent of whether the assumed cosmic ray nucleus entered the detector through the front or back window or through a side wall.

Several alternatives to the standard event requirements are available by command. In the "source mode" the ECL recognizes either a standard event or an event due to an alpha particle or fission fragment from the internal radioactive calibration sources located in ion chambers 2 and 5. Events due to an internal source are characterized by an LLD from chamber 2 in anti-coincidence with the LLD of chambers 1 and 3, or by LLD5 in anti-coincidence with LLD4 and LLD6. The "source mode" was used extensively during ground testing before launch, and in flight this mode is activated by command for about 1 orbit every two weeks. The fission fragments give the only simple test of the stability of the ionization chamber's response to ionization levels well above those produced by cosmic ray iron nuclei. The upper fission peak gives a signal approximately equal to that of a minimum-ionizing cosmic ray nucleus of charge 60 traversing perpendicular to the electrodes.

By command the requirement for two-of-seven "charge detectors" can be changed to one-of-seven. The spacecraft's stored-command processor is used to implement this one-of-seven mode regularly at low event rate parts of the orbit, when the vertical geomagnetic cutoff is above about 12 GV. Since the nuclear charge threshold of the Cherenkov discriminator is significantly below that of the ionization chamber LLD, the effect is to lower the instrument's charge threshold from $Z \simeq 17$ to $Z \simeq 12$ for vertically incident $\beta = 1$ particles.

Several other commands are available, chiefly for the purpose of overriding malfunctioning inputs to the ECL. These permit disabling inputs from any of the charge detectors or enabling inputs from individual X or Z hodoscope layers.

Events, other than those from the fission source, are labeled as "priority" if at least one HLD is triggered, or if at least one ILD and the C2 are triggered. The ILD · C2 insures priority for all events with $Z > 33$ and energy above about 350 MeV/amu, while the HLD insures priority for all events with $Z > 44$ regardless of energy. In fact, most of the priority events are iron ($Z = 26$) or nickel ($Z = 28$) nuclei which triggered an ILD or HDL by virtue of having moderately low energy and/or large angle with respect to the instrument axis. The ILD and HLD thresholds were set so that the rate of priority events is low enough to permit telemetry of these events with nearly 100% efficiency throughout the orbit.

The coincidence resolving time of the ECL for normal events is 26 μs, dictated principally by the time constants of the hodoscope amplifier-discriminators. For priority events the hodoscope signals are necessarily far above threshold and the resulting faster trigger permits a shorter resolving time of approximately 10 μs.

3.5 Data Readout

For each event 464 bits are recorded in a primary buffer including fourteen 12-bit pulse heights, eight 32-bit hodoscope address/patterns, 27 bits indicating discriminator inputs to the ECL, a priority bit, a parity bit, a bit indicating a pulser-calibration event, 6 bits reserved for a calibration pulse code, two bits indicating one or more repeated transmissions of the same event, and a bit indicating the output buffer. In the absence of priority events, normal events are handled in the following manner. An event is held in the primary buffer until one of two output buffers is available, at which time it is transferred to that output buffer and the primary buffer is reset, thus becoming available

to accept another event. The spacecraft reads the output buffers in turn, emptying one output buffer during each spacecraft minor frame, at a rate of one minor frame every 0.32 sec. As each event is transferred serially out to the spacecraft, it is fed back into the output buffer. After being read out once, the buffer is "available" to accept a new event, but if no new event appears in the primary buffer before the next spacecraft readout of that output buffer, the same event is re-transmitted.

For priority events the buffer system operates in nearly the same manner as for normal events except that normal events stored in buffers are ignored by priority events. Thus the primary buffer is "available" for accepting a priority event unless it is holding another priority event. An output buffer is "available" for accepting a priority event unless that buffer is in the process of shifting data to the spacecraft or it is holding another priority event that has not been transmitted; a normal event in an output buffer can be written over by a priority event. An output buffer holding a priority event is "available" to a normal event only after the priority event has been transmitted twice. The result of this system is that nearly all priority events are transmitted at least once, and most of them are transmitted at least twice.

The recording efficiencies (or live times) for normal events and for priority events during any time interval are determined by comparing the number of transmitted events of each kind with the total. The total numbers for each type are registered in two rate scalers, one which scales every event that occurs regardless of the state of the data buffers, and another which similarly records every priority event. These rate scalers are read out and

reset at a fixed time in each major frame (i.e., every 128 minor frames or 40.96 sec).

The event rates and the recording efficiency for normal events vary strongly with location of the spacecraft due to the geomagnetic cutoff, and vary weakly with the orientation of the spacecraft relative to the local zenith. At the highest geomagnetic cutoffs, where the total event rate is typically 1.4/sec and the priority rate is 0.15/sec, the normal event recording efficiency is typically 91% while the priority events are recorded with essentially 100% efficiency. At the lowest cutoffs, where the total event rate is typically 13/sec and the priority event rate is 1.3/sec, the normal event efficiency is typically only 10%, while the efficiency for priority events is 97%. In the central part of the South Atlantic Anomaly, where most events are accidental coincidences, the total event rates reach levels as high as 50/sec.

3.6 Housekeeping

In addition to the event rates described above, a number of other rates are scaled in each major frame: radioactive source rate in each module (e.g., rate of LLD2 in anti-coincidence with LLD1 and LLD3; the hodoscope discriminator rates in each module; the two LLD rates not in the source-chamber in each module (e.g., LLD1 or LLD3); singles rate in each PMT; the rate of two-fold (C2 signals) and four-fold coincident PMT signals.

Analog housekeeping monitors transmitted in each major frame include temperatures on all sides of the ionization chamber modules, at each PMT, and at key points in the electronics, and temperature differences across the

ionization chamber modules. In orbit the typical detector temperatures have ranged between 13° and 21°C. The insulation and thermal mass are such that no variation (< 0.2°C) occurs during an orbit. The most rapid changes observed are about 0.6°C/day, but typically the changes have been much slower. The temperature variations have been dominated by changes in the proportion of an orbit spent in sunlight (due to variations in the angle between the Earth-Sun line and the plane of the spacecraft's orbit). Variations in the temperature difference between the opposite sides of either ionization chamber module have not exceeded 0.2°C.

Analog monitors of the gas pressure in each ionization chamber module have displayed good correlation with the temperature, indicating no detectable change in the gas density to within 0.2%.

4. Performance

The typical response in orbit of the ionization chambers to iron nuclei has been essentially constant with time, exhibiting maximum variations of signal amplitude less than 0.2%. The Cherenkov counter response has exhibited measurable temporal variations, with the mean of the eight PMT signals varying over a range of 5% and variations in the gain of the individual PMT's ranging from about 3% to 7%. The variations are well correlated with temperature changes, although showing small hysteresis effects, and can be explained as thermal effects on PMT gains ranging from ≈ 0.5 to 1%/°C. These gain changes are slow, as are the temperature changes; the fastest observed change on any tube to date has been about 0.5%/day. The response to iron nuclei can be determined to better than 0.15% with data from just one day, so the gain variations can easily be removed in the data analysis.

The areal response of each of the six ionization chambers is quite flat. No non-uniformity ($\gtrsim$ 0.1%) is detected over a rectangular region 40 cm x 70 cm at the center (i.e., > 44 cm from the walls). Outside this region the response falls approximately linearly to 98% of the central response at 8 cm from the walls, with larger variations near the walls.

The areal response of the Cherenkov counter is much less uniform, exhibiting strong peaks in the light collection efficiency near each PMT (Fig. 8). The mean of the eight PMT's is reasonably uniform over the central third of the area; this region, which is more than 25 cm from any PMT, shows variations of about 10% with typical gradients of about 0.2%/cm. The peaks in the response, about 10 cm in front of each pair of PMT, are a factor of about 1.4 above the central region, and near these peaks the gradient reaches about 1.5%/cm; however, by appropriate weighting of the responses of the individual PMT's these gradients can be reduced by a factor of at least three. By accumulating data over three to four month periods so as to get adequate statistics in small areas, we can determine areal response corrections good to 0.5%.

That the telescope can resolve individual charges during flight is illustrated in Figs. 9 and 10 which show charge spectra obtained for nuclei in the $_{14}Si$–$_{28}Ni$ range and for the $_{26}Fe$–$_{30}Zn$ range from data that has not been fully corrected. Clearly individual elements can be resolved even in this case except when there is an extreme disparity between neighboring abundances. In each figure, the iron peak is characterized by a standard deviation of about 0.34 charge units, a figure of merit that should improve as further corrections are applied.

Acknowledgements

The design, fabrication and testing of an instrument such as this is the product of the dedicated efforts of a large number of people, only some of whom can be recognized by name. However, we must thank for engineering assistance, V.M. Noble, W.A. Gneiser, H.A. Chameroy and C. Springer of BASD, J.W. Epstein of WU, W.G. Blodgett of CIT and W. Erickson, G. Peterson and R. Howard of UM. Management of this program was under NASA Marshall Space Flight Center and we acknowledge with thanks the continued assistance of personnel at that Center. The excellent performance of the HEAO spacecraft owes much to the personnel of TRW to whom we are deeply indebted. Funding for this instrument was supported in part by NASA under Contracts NAS8-27976, 7, 8 and grants NGR 05-002-160, 24-005-050 and 26-008-001.

References

1. E.K. Shirk and P.B. Price, Ap.J. 220, 719 (1978).

2. P.H. Fowler, C. Alexander, W.M. Clapham, D.L. Henshaw, D. O'Sullivan and A. Thompson, 15th Intn'l CR Conf. Plovdiv 11, 165 (1977).

3. M.H. Israel, P.B. Price and C.J. Waddington, Physics Today 28, (5) 23 (1975).

4. P.H. Fowler, W.M. Clapham, D.L. Henshaw, A. Thompson and D. O'Sullivan, 16th Intn'l CR Conf. Kyoto 1, 370 (1979).

5. J.P. Meyer, 16th Intn'l CR Conf. Kyoto 1, 374 (1979).

6. J.W. Epstein, J.I. Fernandez, M.H. Israel, J. Klarmann, R.A. Mewaldt and W.R. Binns, Nucl. Inst. and Meth. 95, 77 (1971).

7. J.D. Sullivan, Nucl. Inst. and Methods 95, 5 (1971) Ibid. 98, 187 (1972).

8. P.L. Love, J. Tueller, J.W. Epstein, M.H. Israel and J. Klarmann, Nucl. Inst. and Meth. 140, 569 (1977).

9. W.N. English and G.C. Hanna, Can. J. Phys. 31, 768 (1953).

10. E.K. Hyde, The Nuclear Properties of the Heavy Elements, Vol. III, Fission Phenomena, Prentice-Hall, Inc. (1964).

11. R. Brandt, S.G. Thompson, R.C. Gotti and L. Phillips, Phys. Rev. 131, 2617 (1963).

12. W.R. Scarlett, Ph.D. Thesis "An Experimental Study of the Chemical Composition of the Heavy Cosmic Ray Nuclei" University of Minnesota (1977).

Table 1

A. Flight Instrument Materials

1. Aluminum (various alloys)
2. Stainless steel (various alloys)
3. Vespel polyimide (SP-1)
4. Mylar (type A) polyester
5. PR-1660 polyurethane adhesive
6. Glass
7. Copper
8. Gold
9. Platinum
10. Californium

B. Other Materials Tested

1. Mycalex 410
2. FM 96U adhesive
3. Epon 828-TETA adhesive
4. Epon 828-versamid 125

Fig. 1. A schematic view of the particle telescope. From the top this diagram shows hodoscope H1, ion chambers, IC3, IC2 and IC1, H2, Cherenkov radiators 1 and 2, H3, IC6, IC5, IC4 and H4.

Fig. 2. Geometry factors resulting from four different selection modes. A, H1:H4 mode; B, H1:H3:$\overline{H4}$ and H4:H2:$\overline{H1}$; C, H1:H2:$\overline{H3}$ and H4:H3:$\overline{H2}$; D, $\overline{H1}$:H2:H3:$\overline{H4}$. (a) Integral factors in $m^2 \cdot sr$, (b) differential in $cm^2 \cdot sr$ for 2° intervals.

Fig. 3. Voltage and pressure dependence of the ion chamber charge signal for 6.1 MeV alpha particles and ~ 100 MeV fission fragments from ^{252}Cf. The expected dependence of the electron drift velocity is also shown.

Fig. 4. Overall block diagram of the electronics. Each signal is coupled to an amplifier through a charge sensitive preamplifier. Pulse height analyzers (PHA) and discriminators (DISC) provide the digital input to the control logic and data buffers.

Fig. 5. Map of correction factors for the sum of the responses of the 8 Cherenkov photomultiplier tubes, two of which are located in each of the four corners. The map is circumscribed by the outline of the Cherenkov radiator and is normalized to unity at the center.

Fig. 6. A charge spectrum for the abundant lower charged nuclei. This spectrum comes from a selected set of data obtained early in the mission and is uncorrected for any systematic biases.

Fig. 7. A charge spectrum of the elements just heavier than iron. Note the logarithmic abundance scale. The same cautions as on Fig. 6 are applicable.

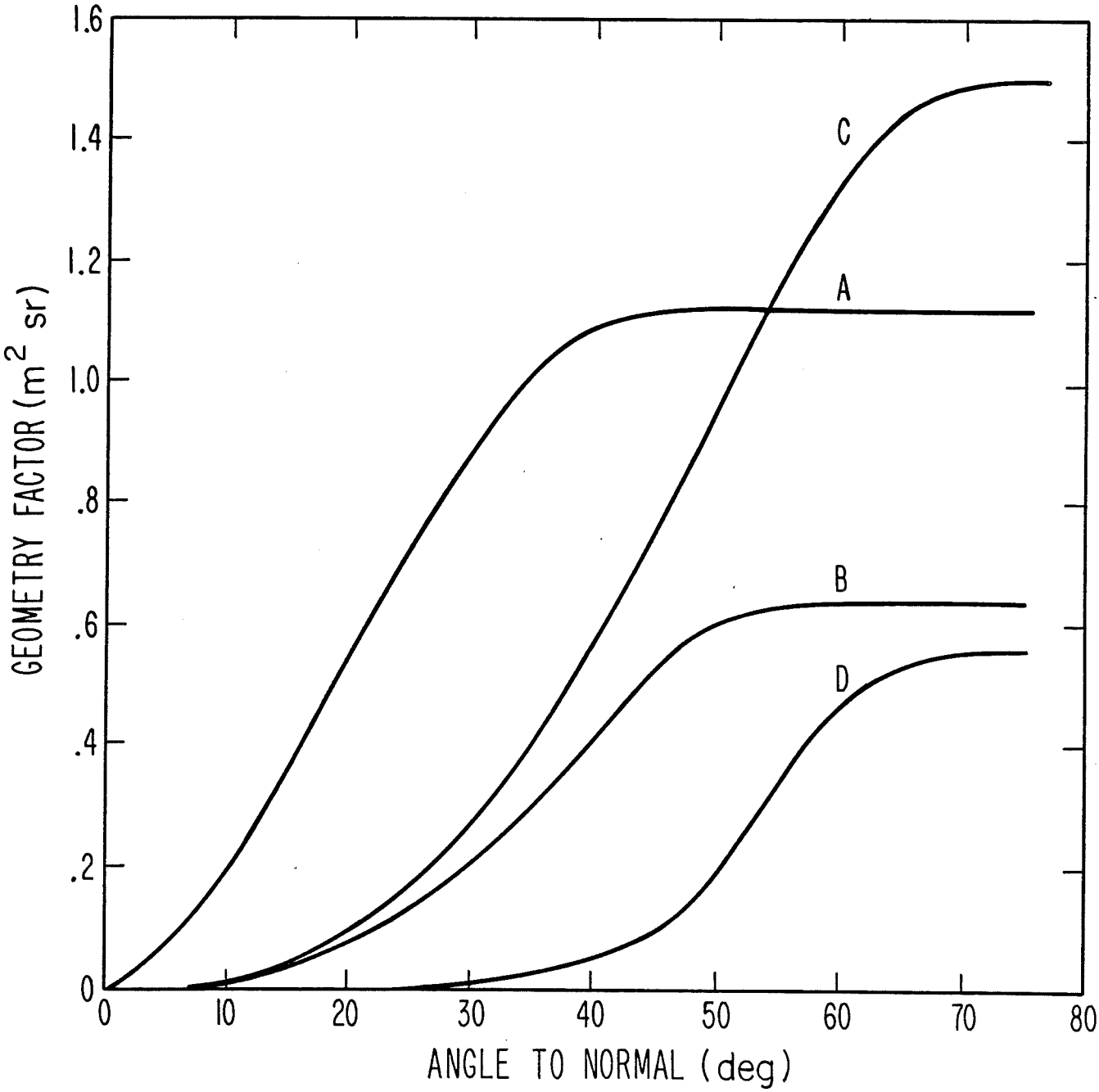
1.6
1.4
1.2
1.0
.8
.6
.4
.2
0
GEOMETRY FACTOR (m^2 sr)
0
10
20
30
40
50
60
70
80
ANGLE TO NORMAL (deg)
A
B
C
D

Figure 1.

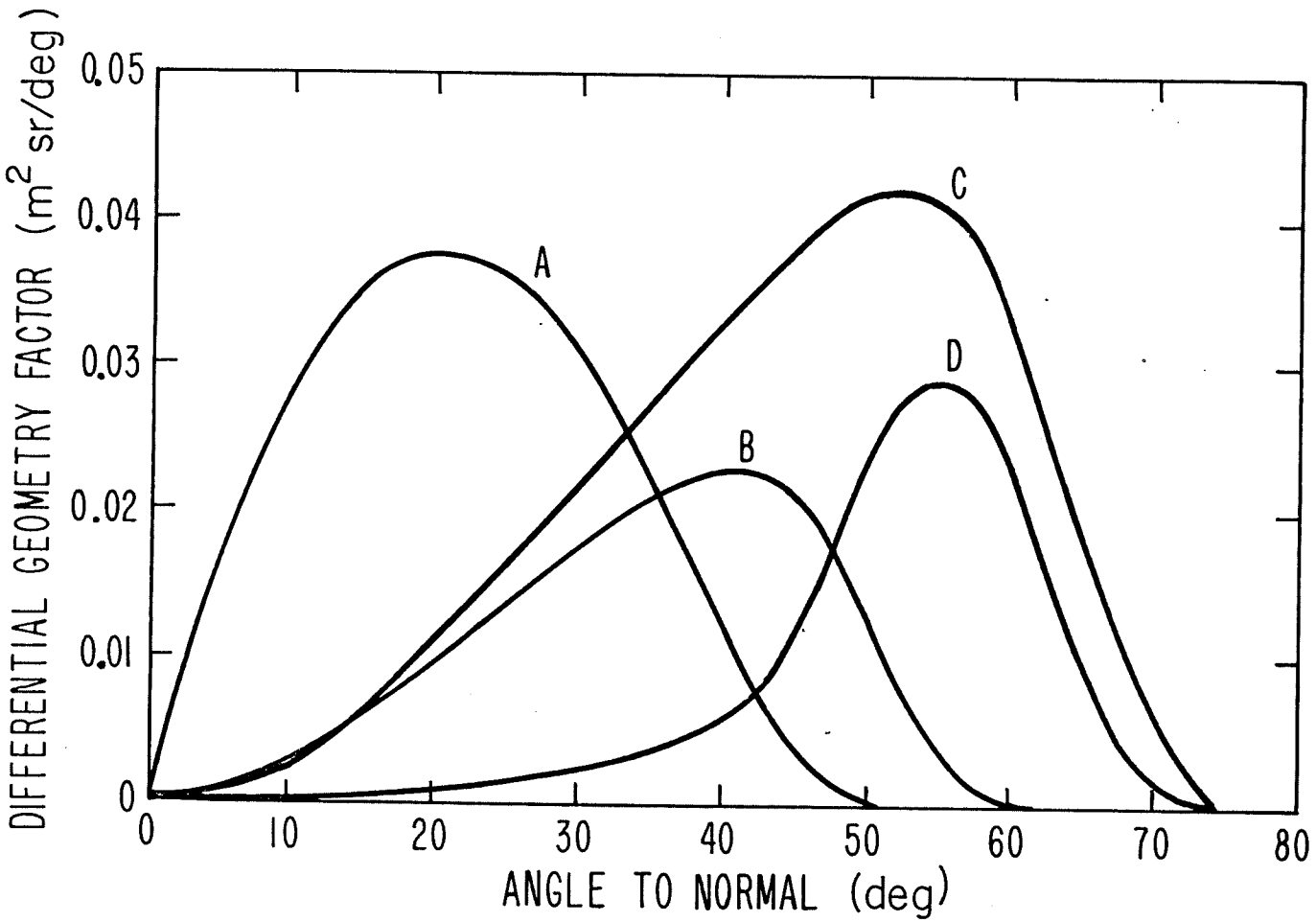
DIFFERENTIAL GEOMETRY FACTOR (m^2 sr/deg)
0.05
0.04
0.03
0.02
0.01
0
A
B
C
D
0
10
20
30
40
50
60
70
80
ANGLE TO NORMAL (deg)

Figure 2.

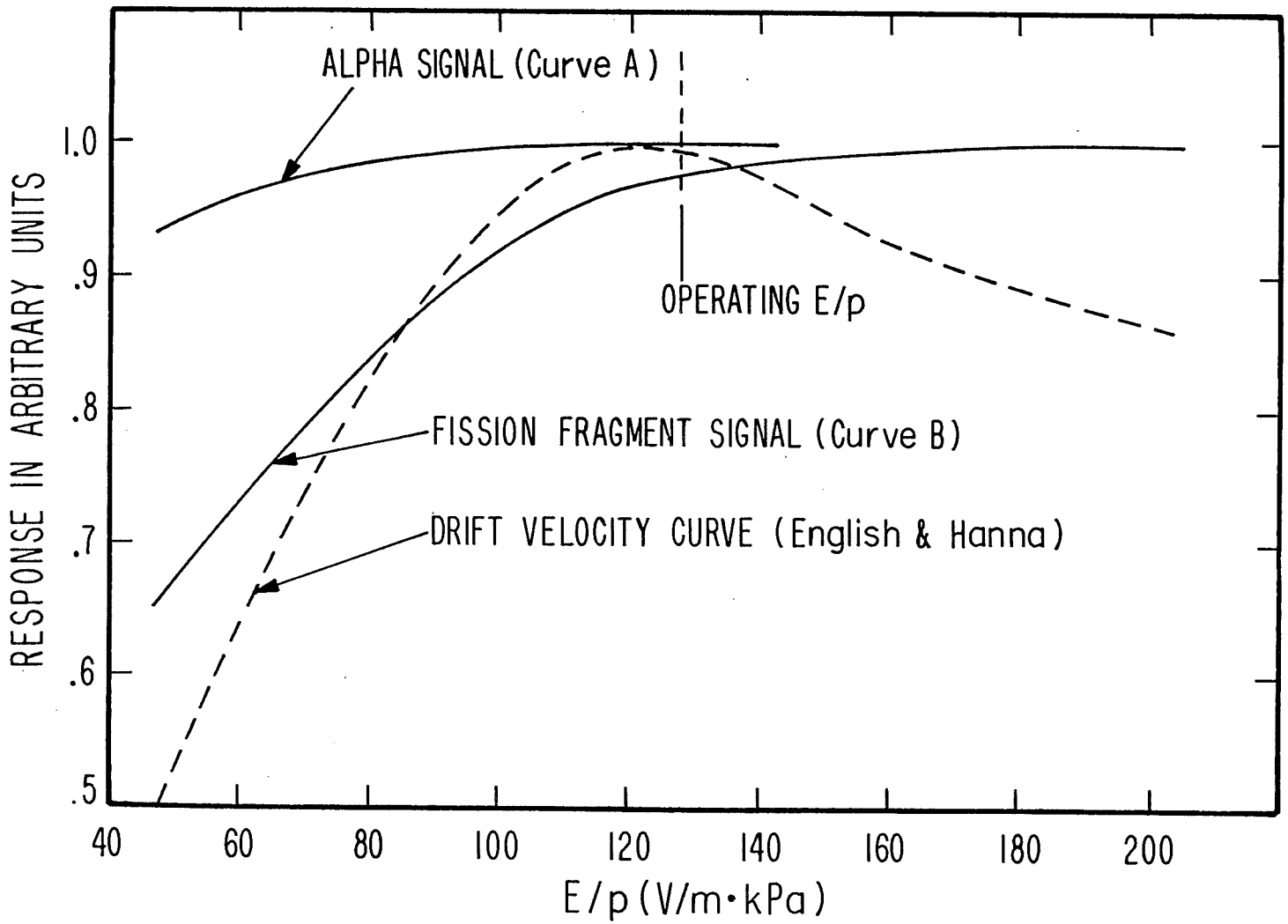
ALPHA SIGNAL (Curve A)
OPERATING E/p
FISSION FRAGMENT SIGNAL (Curve B)
DRIFT VELOCITY CURVE (English & Hanna)
RESPONSE IN ARBITRARY UNITS
1.0
.9
.8
.7
.6
.5
40
60
80
100
120
140
160
180
200
E/p (V/m·kPa)

Figure 3.

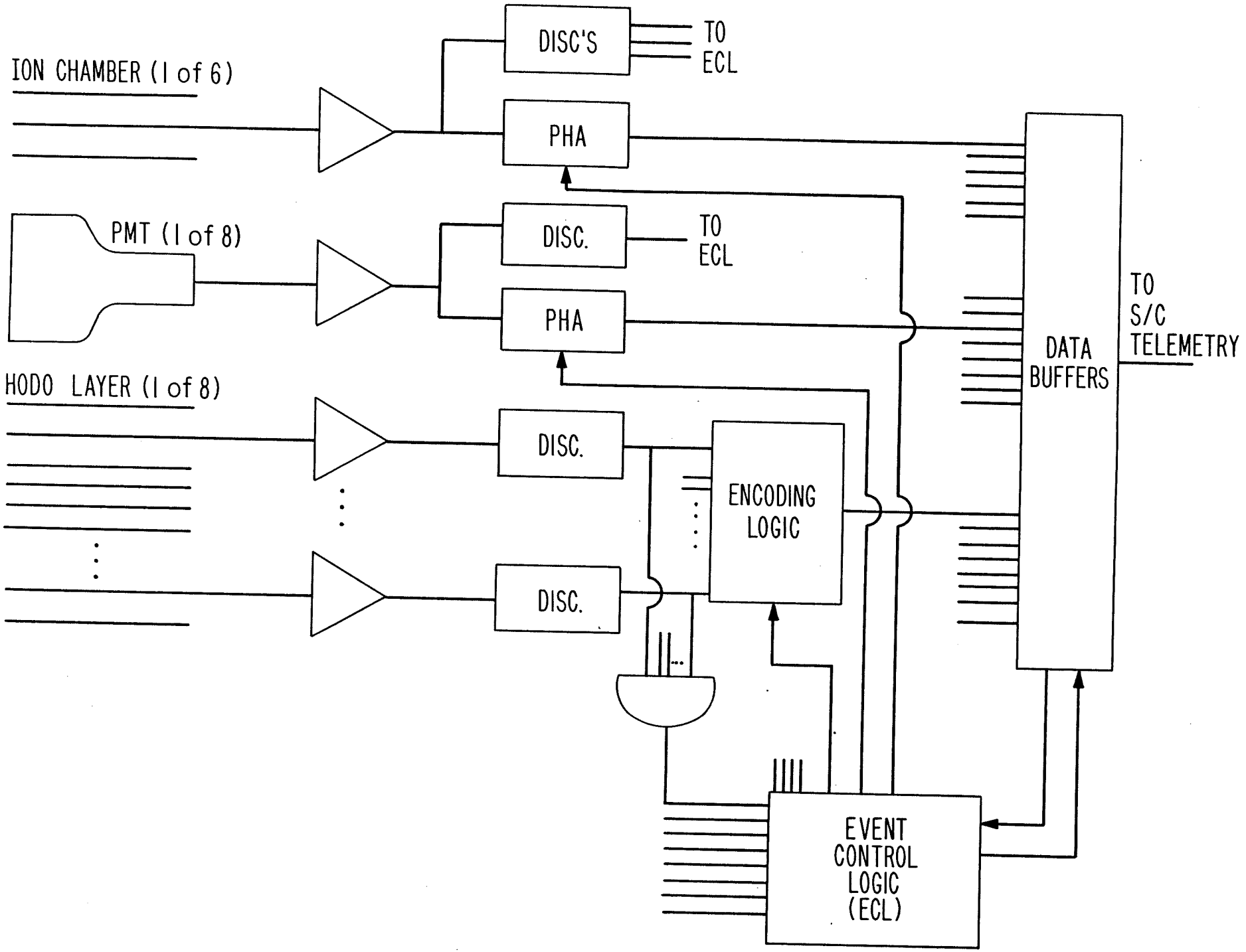
ION CHAMBER (1 of 6)
PMT (1 of 8)
HODO LAYER (1 of 8)
DISC'S
TO ECL
PHA
DISC.
TO ECL
PHA
DISC.
DISC.
ENCODING LOGIC
DATA BUFFERS
TO S/C TELEMETRY
EVENT CONTROL LOGIC (ECL)

Figure 4.

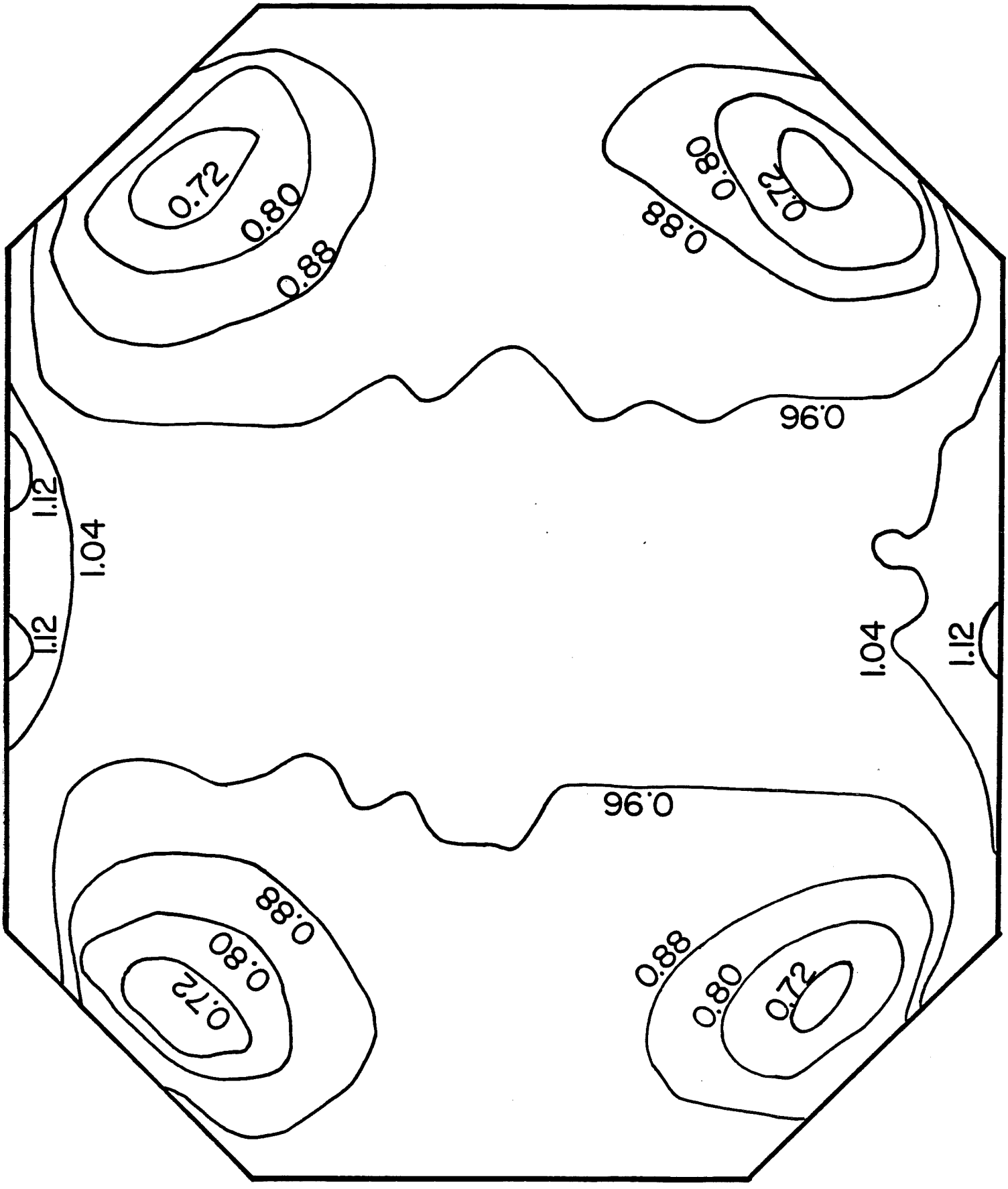
0.72
0.80
0.88
0.72
0.80
0.88
0.96
1.12
1.04
1.12
1.04
1.12
0.96
0.88
0.80
0.72
0.88
0.80
0.72

Figure 5.

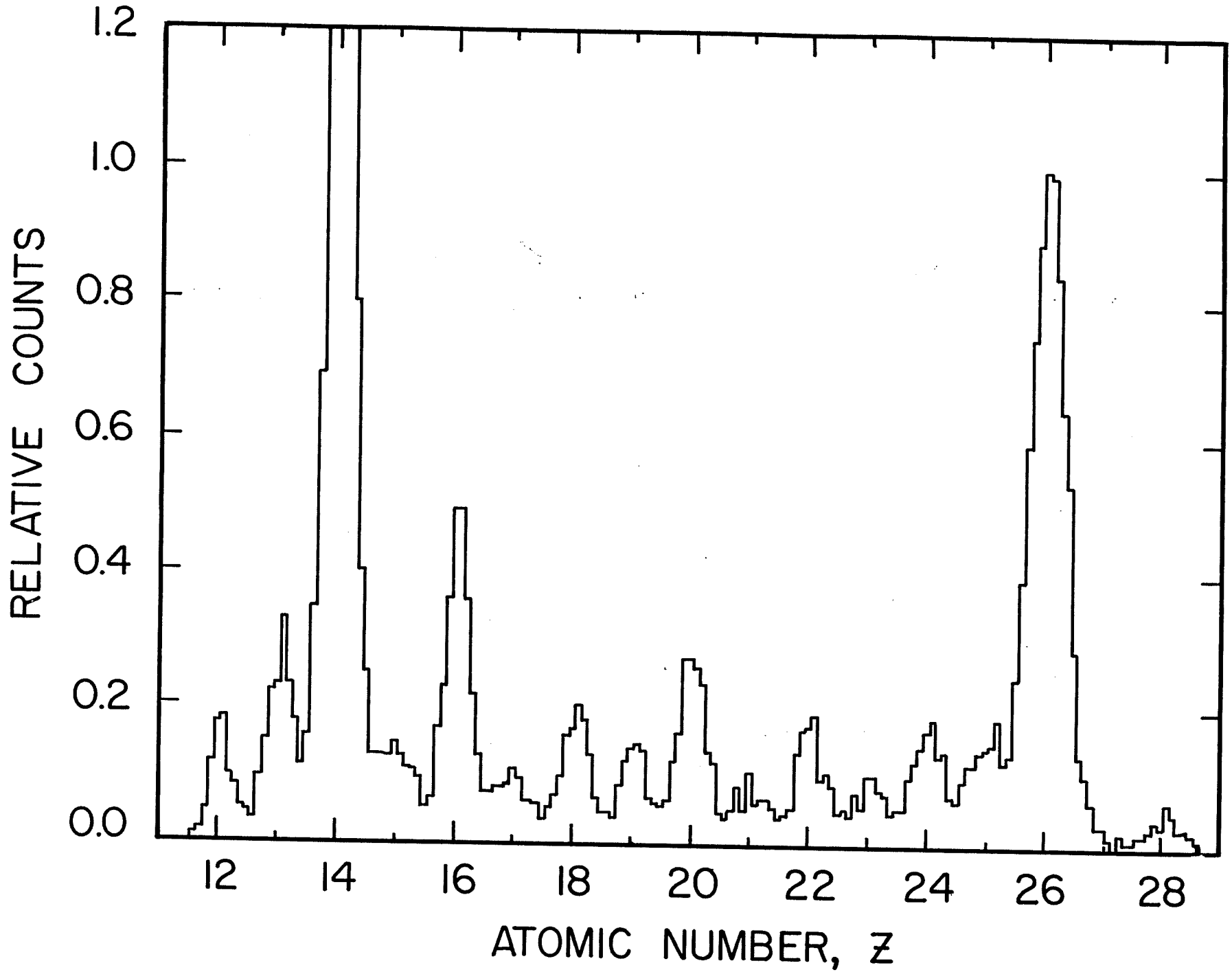
RELATIVE COUNTS
1.2
1.0
0.8
0.6
0.4
0.2
0.0
12
14
16
18
20
22
24
26
28
ATOMIC NUMBER, Z

Figure 6.

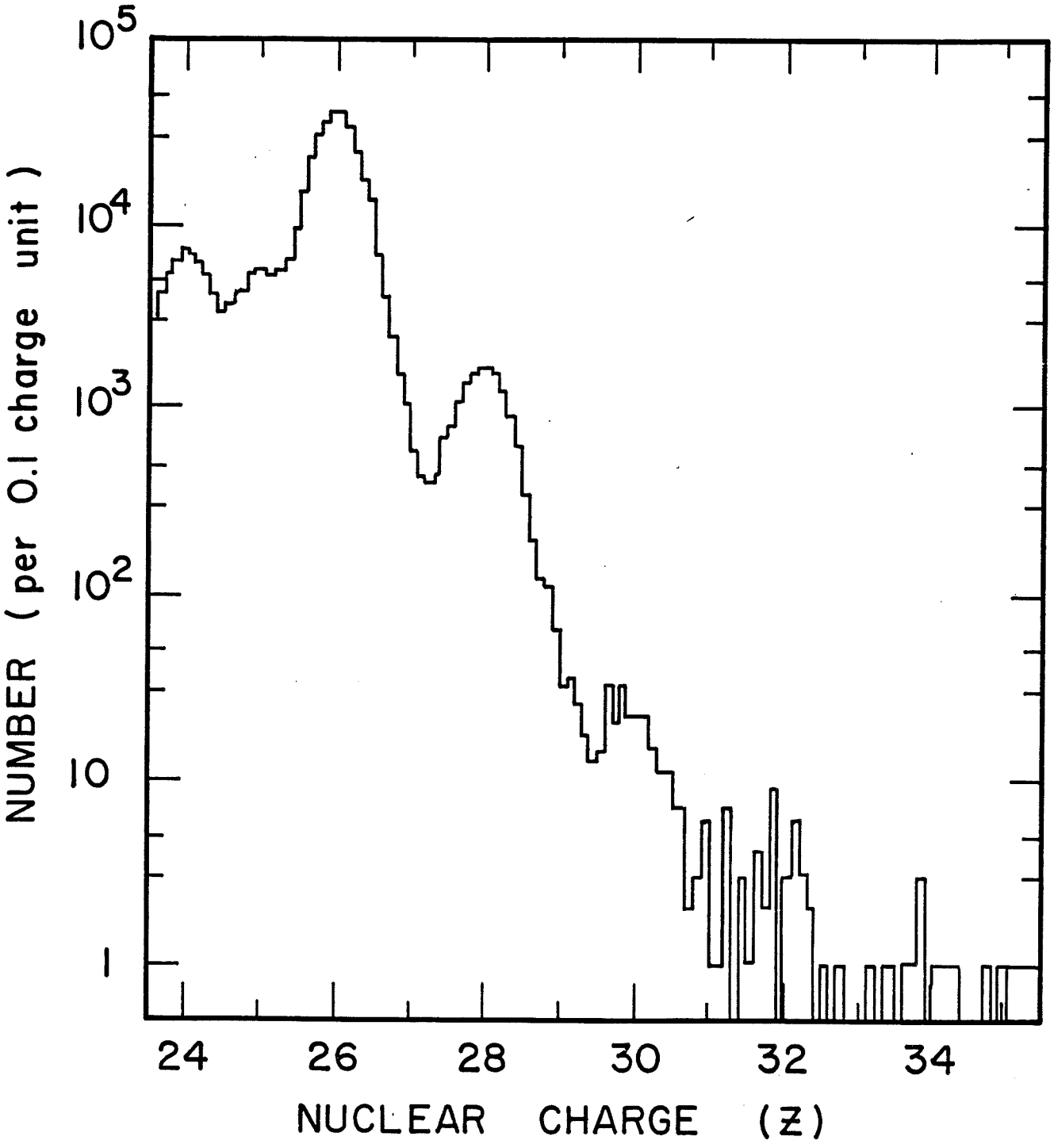
10^5
10^4
10^3
10^2
10
1
NUMBER (per 0.1 charge unit)
24
26
28
30
32
34
NUCLEAR CHARGE (Z)

Figure 7.

ERRATUM

"The UH-Nuclei Cosmic Ray Detector on the Third High Energy Astronomy Observatory"

W.R. Binns, M.H. Israel, J. Klarmann, W.R. Scarlett,
E.C. Stone, and C.J. Waddington

Figure 1 was not included in the preprint. The drawing labeled Figure 1 is actually Figure 2a and drawing labeled Figure 2 is actually Figure 2b. Figure 1 is given below. The figure captions are correct.

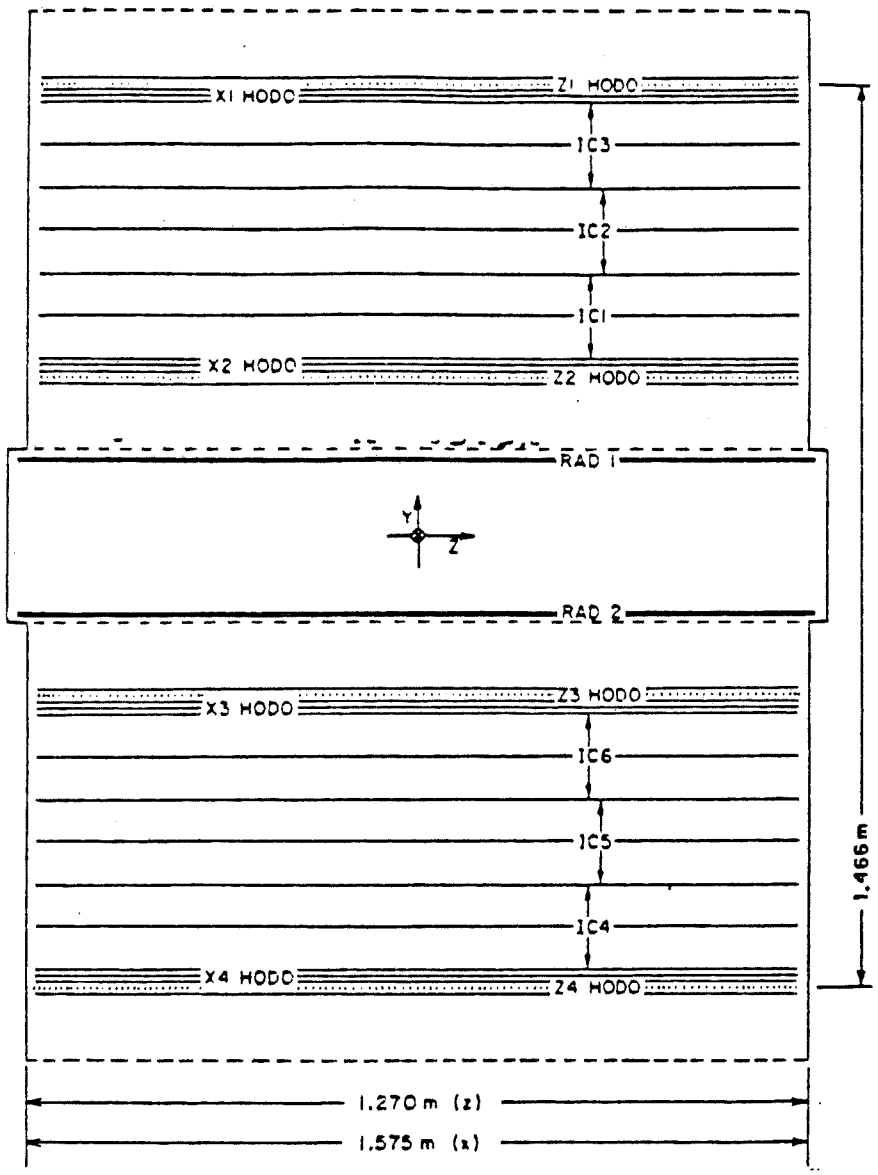

Figure 1.